Accepted Manuscript

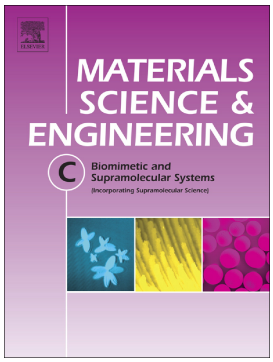

New design of highly sensitive AIE based fluorescent imidazole derivatives: Probing of sweat pores and anti-counterfeiting applications

M.K. Ravindra, K.M. Mahadevan, R.B. Basavaraj, G.P. Darshan, S.C. Sharma, M.S. Raju, G.R. Vijayakumar, Kiran B. Manjappa, Ding-Yah Yang, H. Nagabhushana

PII: S0928-4931(18)33458-1
DOI: https://doi.org/10.1016/j.msec.2019.03.089
Reference: MSC 9598

To appear in: *Materials Science & Engineering C*

Received date: 11 November 2018
Revised date: 13 March 2019
Accepted date: 24 March 2019

Please cite this article as: M.K. Ravindra, K.M. Mahadevan, R.B. Basavaraj, et al., New design of highly sensitive AIE based fluorescent imidazole derivatives: Probing of sweat pores and anti-counterfeiting applications, Materials Science & Engineering C, https://doi.org/10.1016/j.msec.2019.03.089

This is a PDF file of an unedited manuscript that has been accepted for publication. As a service to our customers we are providing this early version of the manuscript. The manuscript will undergo copyediting, typesetting, and review of the resulting proof before it is published in its final form. Please note that during the production process errors may be discovered which could affect the content, and all legal disclaimers that apply to the journal pertain.

ACCEPTED MANUSCRIPT

New design of highly sensitive AIE based fluorescent imidazole derivatives: Probing of sweat pores and anti-counterfeiting applications

M. K. Ravindra[1], K. M. Mahadevan[1], R.B. Basavaraj[2], G.P. Darshan[3], S.C. Sharma[4], M.S. Raju[5], G.R. Vijayakumar[6], Kiran B. Manjappa[7], Ding-Yah Yang[7], H. Nagabhushana[2,*]

[1]Department of Chemistry, Kuvempu University, P. G. Centre, Kadur 577 548, India
[2]Prof. C.N.R. Rao Centre for Advanced Materials Research, Tumkur University, Tumkur 572 103, India
[3]Department of Physics, Acharya Institute of Graduate Studies, Bangalore 560 107, India
[4]National Assessment and Accreditation Council, Bangalore 560072, India (Work carried out as honorary Professor, Jain University, Bangalore 562112, India)
[5]Department of Physics, Smt & Sri Y.E. Rangaiah Setty Govt. First Grade College, Pavagada 561 202, India
[6]Department of Chemistry, University College of Science, Tumkur University, Tumkur 572 103, India
[7]Department of Chemistry, Tunghai University, No. 1727, Sec. 4, Taiwan Boulevard, Xitun District, Taichung, 40704, Taiwan

Abstract

A novel aggregation induced emission based 2-(1-(3, 5-bis(trifluoromethyl)phenyl)-4,5-diphenyl-*1H*-imidazol-2-yl) phenol (4) (IMD) fluorescent tags (FTs) was designed by simple acid catalyzed five-member N-heterocyclic ring forming reaction process. Powder X-ray diffraction results showed mechanofluorochromic properties of IMD FTs are easily reversible under external force due to the decrease in crystallinity. These IMD FTs also exhibits strong cyan-blue luminescence in solid state with high quantum efficiency. Detailed investigation of latent fingerprints (LFPs) showed permanent, immutable and unique pores that are distributed on the ridges. The visualization of such sweat pores opens new avenue in the field of forensic science. Hence, the prepared IMD FTs exhibit excellent Lipophicity (LP) properties, which endorse its possible applications for the visualization of sweat pores present in the LFPs. The LFPs visualized by IMD FTs exhibit excellent efficiency, sensitivity, selectivity, low background hindrance and less toxicity. The obtained result evident that the prepared FT and followed technique opens possible applications for the visualization of LFPs on various porous/semi-porous/non-porous surfaces under UV 365 nm light.

Keywords: Aggregation induced emission; Latent fingerprint; Powder staining technique; Photoluminescence; Sweat pores.

* Corresponding author: +91- 9945954010, E-mail address: bhushanvlc@gmail.com (H. Nagabhushana)

ACCEPTED MANUSCRIPT

1. Introduction

The design and synthesis of emissive π-conjugated solid-state luminophores has attains tremendous interest due to their broad application in various fields, such as organic light emitting diodes (OLEDs), bio-imaging, organic solid-state lasers (OSSLs) and sensors. For full-color display, the blue emitter was most significant because it reduces the power consumption, however it can also be used to produce light of some other colors by energy cascade to a lower-energy fluorescent or phosphorescent dopants [1-3]. Therefore, the blue OLEDs with low cost, high efficiency have been required to launch the commercialization [4]. In this regard, nitrogen containing heterocyclic compounds with strong electrons acceptor derivatives found to be highly efficient, which opens to the wide spread of applications [5, 6]. Further, these compounds were utilized as a chromosphere due to its higher extinction coefficient, absorption wavelength fluorophore and readily tunable properties [7].

For past decades, the LFPs were most evidential investigative tool for personal identification and bio-metric systems [8-11]. Generally, Level 1 & 2 ridge details of fingerprints (FP) can be easily counterfeited by artificial skin imprints. However, level 3 ridge details provide more noteworthy discriminatory details for FPs matching and have additional impact on probing of age, ethnic origin, medication, psychological state, health, metabolism, etc. [12]. Till date, many techniques have been followed for visualization of LFPs, including powder staining, spraying chemical reagents, iodine fuming, ultraviolet/visible, fluorescence, infrared, Raman spectroscopy techniques, etc. [13-20]. Jin et al., [21] visualized the LFPs by aggregation-induced emission (AIE) based tetraphenylethene (TPE) by following spraying method under UV light. The results were restricted to level 1 and 2 ridge details including arches, tented arches, loops, double loops, whorls, eyes, bifurcations, line fragments and endings of finger-lines. Liu et al visualized LFPs on various surfaces by using AIE-active heteroleptic Ir (III) complex. They summarized up to level 3

ACCEPTED MANUSCRIPT

ridge characteristics except sweat pores [22, 23]. Therefore, visualization of level 3 details (sweat pores) present in the fingerprints accelerate researchers to perform further work.

Information security was a key issue in daily life, economic, social and military fields. Hence, the development of new materials for anti-counterfeiting has gathered much consideration for their use in protection and detection of counterfeiting. From past decades, numerous technologies have been developed for information security namely markers, plasmonic labels, magnetic labels, holograms and luminescence materials. Among these, the luminescence materials, such as carbon dots, semiconductor dots, rare earth doped nanophosphors, organic dyes, etc. have been widely used for anti-counterfeiting and data encryption applications due to its visibility, high throughput and facile design advantages [24-29]. In addition, luminescent materials were invisible upon normal light excitation; however, they were highly visible under multiple excitations. Hence, such materials can be well-designed for anti-counterfeiting applications. Although, there are many materials have been reported as luminescent security ink but they have their own disadvantage like toxicity, broad emission and solubility in harmful solvent. The formation of stable and transparent solution of these nanoparticles is also a difficult task. Therefore, the fabrication of eco-friendly luminescent tags was crucial [30, 31].

In the present work, a novel blue light emitting IMD FTs were prepared by simple route as described in scheme 1. The structural, morphological, mechanofluorochromic (MFC), photoluminescence (PL), photometric and LP properties of the IMD FTs was extensively studied. Based on the obtained results, prepared IMD FT can be explored as a fluorescent labelling agent for the visualization of unique sweat pores on various surfaces and security ink applications.

ACCEPTED MANUSCRIPT

2. Experimental

2.1. Synthesis of IMD FT

3,5-bis-trifluoro-methyl aniline (1 mmol, 0.229 g), benzil (1 mmol, 0.210 g), ammonium acetate (1 mmol, 0.75 g) and salicylaldehyde (1mmol, 0.122 g) were mixed in a single necked round bottom flask containing glacial acetic acid (20 mL). The reaction mixture was subjected to ultrasonication for ~ 10 -20 min and kept for reflux for ~ 5 h. The progress of reaction was monitored by thin layer chromatography (TLC) using *n*-hexane: ethyl acetate mixture (7:3). After completion of the reaction, the mixture was cooled to room temperature (RT) and poured into 100 mL of ice cold water. The resultant solution was neutralized by aqueous sodium bicarbonate and product was extracted with ethyl acetate (50 mL × 3). The combined organic layer was removed by using a rotary evaporator under reduced pressure resulted a desired product. The crude product was then recrystallized by a hot acetic acid to obtain fine crystals of analytically pure IMD FTs. White crystalline solid; Yield: 80 %; mp: 210-212 °C; IR (KBr) (v_{max}/cm^{-1})): 1385.92 (C-F), 1588.89 (Ar C=C), 1601.92 (C=N), 3055.53 (Ar C-H), 3435.40 (Phenolic O-H); ^{1}H NMR (400 MHz, DMSO-d_6, (ppm)): δ = 6.758-6.823 (m, 2H, Ar-H), 7.12-7.15 (m, 1H, Ar-H), 7.17-7.25 (m, 2H, Ar-H), 7.25-7.35(m, 4H, Ar-H), 7.335-7.356 (m, 3H, Ar-H), 7.47-7.50 (m, 2H, Ar-H), 7.85 (s, 2H, Ar-H), 8.036 (s, 1H, Ar-H), 10.761 (s, 1H, Phenolic OH).

2.2. Characterization

Powder X-ray diffraction (PXRD) patterns were recorded using Shimadzu made X-ray diffractometer with Cu-Kα radiation (λ ≈ 0.15406 nm). Morphology and chemical composition were studied by using Hitachi made (Model No. TM-3000 (SEM) and H-8100 (TEM)) electron microscopes. Perkin Elmer spectrophotometer (λ -35) was used to study the diffuse reflectance (DR) studies of the prepared samples. The photoluminescence (PL) data were recorded using Jobin Yvon Spectroflourimeter Fluorolog-3 operational with Xenon

ACCEPTED MANUSCRIPT

lamp (450 W) as an excitation source. The crystal XRD data was recorded on a Bruker Smart CCD Area Detector System using Mo-Kα (λ ≈ 0.71073 Å) radiation. The data were reduced using SAINT-Plus. The structure was solved by direct methods using SHELXS97 and subsequent ΔF-synthesis. The approximate positions and anisotropic displacement parameters of all hydrogen atoms were found in different stages of the converging structure refinements by means of full-matrix least-square refinement using SHELXL97. Molecular diagrams were generated using ORTEP. The mean plane calculations were estimated using PARST program.

2.3. Visualization of LFPs using IMD FT

The LFPs on various porous (namely, magazine cover, aluminum foil, complex background paper, barcode) and non-porous (namely, computer mouse, glass slide, metal scale, coin and spatula) surfaces are collected from various distinctive donors. Before stamping the LFPs, the volunteer's hands were washed thoroughly with soap water. Then, the prepared IMD FT was stained on the LFPs with a light brushing action. The excess IMD FT was removed by dusting the substrate surfaces with a gentle, smooth motion until a FPs image was developed. The developed FPs image were photographed *in situ* using a DSLR Canon EOS 100D camera with 5 mm focal point (SIGMA MACRO, 50 mm, F2.8, EXDG) under 365 nm UV light. In addition, conventionally used Fe_2O_3 [< 5 μm, ≥ 96 % purity, Sigma-Aldrich] powder was utilized for comparison of the developed FPs.

2.3. Preparation of anti-counterfeiting ink.

A standard PVC gold medium (locally fabricated, printing ink manufactured by Commercial Techno Colors, Ram Nagar, Varanasi-221 005, India) was used to disperse the IMD FTs. The dispersive medium provides better dispersion of FTs into the medium without any clusters and achieving higher viscosity (3000 micro poise), which offers sticky nature with printing paper. In the present work, a commercially purchased 50 ml PVC gold medium solution and 250 mg of IMD FTs were taken in a beaker and sonicated for ~ 1 h to obtain a clear and

ACCEPTED MANUSCRIPT

transparent solution. To make a pattern onto paper, we used a dip pen technique for designing various shapes. Schematic illustration for the LFPs visualization and anti-counterfeiting applications using IMD FTs were depicted in Fig.1.

3. Results and discussion

3.1. Chemistry

Aggregation induced emission based IMD FTs was designed by simple acid catalyzed five-member N-heterocyclic ring forming reaction process. The synthetic reaction scheme and proposed mechanism for IMD FT was shown in Fig.2.The systematic proposed mechanism for the preparation of the IMD FT follows four steps, as given below;

Step-1: Benzil reacts with ammonium acetate and forms 2-imino-1,2-diphenylethanone.

Step-2: A lone pair of electron on nitrogen of 2-imino-1, 2-diphenylethanone reacts at imine carbon of Schiff base, which formerly obtained by the condensation of salicylaldehyde and 3,5-bis(trifluoromethyl)aniline to form 2-((3,5-bis(trifluoromethyl)phenylamino)(2-hydroxyphenyl)methylamino)-1,2-diphenylethanone.

Step-3:2-((3,5-bis(trifluoromethyl)phenylamino)(2-hydroxyphenyl)methylamino)-1,2 diphenylethanone undergoes intramolecular cyclization by the reaction of lone pair electrons of nitrogen (NH group) at electron deficient carbon of carbonyl group to form an intermediate.

Step-4: The obtained intermediate undergoes dehydration followed by aromatization to get final IMD FTs.

3.2. AIE feature of IMD FTs

PL emission spectra of IMD FTs in good solvent (THF) with the incremental addition of poor solvent (H_2O) was shown in (Fig.3 (a)). The spectra exhibit a blue emission intensity centered at ~ 450 nm, which was due to the $\pi^* \rightarrow \pi$ transition and free rotation of the aromatic ring present in it [32]. The variation in the PL intensity with various f_w was also depicted in Fig.3

ACCEPTED MANUSCRIPT

(b). It was evident from the figure that the gradual enhancement in the emission intensity at ~ 452 nm with the increasing of water part (f_w) values from 0 to 70 % was noticed. This PL enhancement was mainly due to two distinctive vital perspectives. They are (i) **Formation of molecular aggregates:** after expanding the water fraction (poor solvable) there is a diminishing in solubility of IMD FT in the THF/H_2O combination because of its inherent hydrophobic nature. This may lead to more intermolecular interactions, which prompts the isolated molecules to involve in the aggregate creation. The aggregation mechanism hindrances the free space accessible for intermolecular rotation and vibration. This confines the rotation of the phenyl rotors and suppresses one of the prevailing non-radiative decay pathways. Subsequently, the excited molecules return to their ground state via fluorescence. (ii) **Common solvent impact:** the molecular absorption in IMD FTs was mainly ascribed to the intramolecular charge transfer (ICT) from the ring nitrogen to the carbonyl moiety [33-36]. Therefore, the supplement of water may enhance the ICT mechanism by balancing the more polar excited state. It's evident that the AIE property depends on the contribution of polar and poor solvation property of water. Conversely, a drastic diminishing nature of emission intensity was observed when f_w value is >70 %, which may be due to diminished dissolvability.

Photographs of the IMD FT dissolved in different solvents, namely DMSO, THF, Acetone and DMF under normal and UV 365 nm light were shown in Fig.4. The obtained results evident that the, IMD FT dissolved in DMSO solvent displays maximum emission intensity in lower f_w solutions and later diminishes (Fig. 4 (a & a^1)). However, IMD FT and THF with f_w = 70 % solution exhibit excellent blue emission with high intensity under UV excitation. Subsequently, similar trend was observed in IMD FT dissolved in Acetone with different f_w under normal and UV 365 nm light and shown in (Fig. 4 (c & c^1)). The weak blue emission intensity was observed in pure solvents, which may have attributed to free rotation

ACCEPTED MANUSCRIPT

of the aromatic rings [37, 38]. A strong blue emission intensity was observed for ~ 50 – 70 % of f_w and thereafter the emission intensity diminishes with the increase of f_w. However, contrasting result was observed in IMD FT dissolved in DMF solvent displays maximum emission intensity in lower f_w solutions and later diminishes (Fig. 4 (d & d^1)).

3.3. DR spectral studies

Fig.5 (a) shows the DR spectra of IMD FT recorded at RT in the range of ~ 200-1100 nm. It was evident that, a strong absorption peak ~ 390 nm was noticed. Further, the energy gap (E_g) of the prepared FT was estimated by using the following relations [39];

$$F(R_\infty) = \frac{(1-R_\infty)^2}{2R_\infty} \text{ ---------- (1)}$$

$$h\nu = \frac{1240}{\lambda} \text{ ---------- (2)}$$

where R_∞ and λ; the reflection coefficient and absorption wavelength, respectively. The plots of $[F(R_\infty)h\nu]^{1/2}$ versus photon energy ($h\nu$) were shown in Fig.5 (b). The E_g value of the prepared samples was found to be 3.11 eV.

3.4. Mechanofluorochromic (MFC) properties

To examine the MFC properties of prepared IMD FTs, solid state PL emission spectra of unground and ground IMD FTs were studied (Fig.6). It was evident that, the spectra exhibit minor variation in emission intensity before and after grinding. In addition, the maximum emission peak at ~ 452 nm show blue-shift after grinding, which indicates MFC properties for the prepared sample. In addition, the quantum efficiency of the IMD FTs in a solid state using PL data was estimated based on the following relation;

$$QE = \frac{Number\ of\ photons\ emitted}{Number\ of\ photons\ absorbed} = \frac{E_c - E_a}{L_a - L_c} \text{ ----------(3)}$$

where, E_c ; the integrated luminescence of the IMD FT caused by direct excitation, E_a ; the integrated luminescence from the empty integrating sphere (blank, without sample), L_a; the

ACCEPTED MANUSCRIPT

integrated excitation profile from the empty integrating sphere, L_c; the integrated excitation profile when the sample is directly excited by the incident beam. In the present case, the QE of the samples were estimated and found to be ~ 76 %. The emission color of the prepared IMD FT was also confirmed by the Commission International de I'Eclairage (CIE) diagram and shown in the inset of Fig.6. The CIE diagram clearly exhibits cyan color emission from the unground sample.

Further, the variation of emission intensity of IMD FTs toward unground, grinding and fuming processes were presented in Fig.7. The initial crystalline sample display a strong blue emission under 365 nm UV light (Fig.7(a)). After adequate grinding by using a mortar, the IMD FT exhibit diminished intensity (Fig.7(b)). Further, the grinded sample could be restored to its original color when fumed by acetone vapor (Fig.7(c)), which suggests that the IMD FT possess MFC and vapochromic properties. The observed MFC property of IMD FT was attributed to destroyed intermolecular interactions and the molecules adopt twisted conformations [40, 41]. The observed blue emission shift after grinding was also supported the decrease of conjugation caused by the twisted conformation [42, 43]. Furthermore, grinding–fuming processes can be performed reversibly many times without fatigue (Fig.7 (d)).

To gain insight into the mechanism of the MFC property, powder X-ray diffraction (PXRD) measurements of IMD FTs in solid states were studied. Fig.8 depicts the PXRD patterns of IMD FT before and after grinding. Intense and sharp diffraction peaks of without ground sample exhibiting highly ordered arrangement of atoms. In contrast, patterns of the grounded sample do not exhibit any noticeable reflection peaks of IMD FT, which entails the formation of amorphous states. When the grounded IMD FT was fumigated with acetone vapor, sharp and intense diffraction peaks were recovered and coincided with those in the initial sample, which suggests the recovery of the ordered crystalline state. Therefore, MFC

ACCEPTED MANUSCRIPT

behaviors should occur because of a phase transition from the crystalline to the amorphous state. To further understand the solid-state properties, single crystals of IMD FT were obtained by solvent evaporation method at RT. The ORTEP structure of IMD FTs was shown in Fig.9. IMD FT crystallized in triclinic crystal system with cell volume of 1133.5(2) $Å^3$ and Z = 2. The detailed crystal data and structure refinement parameters of IMD FT are tabulated in Table 1.

3.5. Morphological analysis

SEM images of the ground and unground IMD FT were displayed in Fig.S1 (a & b)). It was evident that the larger sized particles with agglomeration were observed in unground IMD FT Fig.S1(a)). However, smaller smooth surface morphology was noticed in grounded sample Fig.S1(b)). Further, TEM images of the ground and unground IMD FT were depicted in Fig.S1 (c & d). The obtained results were well agreed with the SEM images. Inset Fig.S1 (c) shows the EDS analysis of the prepared sample which carried out along with TEM analysis. The obtained result confirms the presence of carbon, nitrogen and oxygen groups. The atomic percentage of these groups was equal to 100 %. The obtained results were well agreement with the XRD structure of the prepared IMD FT (Fig.9).

3.6. Lipophicity study

To investigate the LP among the fatty residues of LFPs and IMD FT, a PL emission spectra was recorded when LFPs were stained by IMD FT on various surfaces, namely glass, plastic, paper and steel (Fig.10). The apparent blue-shift (~ 18 nm) in IMD FT deposited LFPs regions as associated with those of without stain samples shows the existence of interactions between the IMD and fatty residues of the LFPs. The obtained results validate that the fatty acid residue can change the LP property of IMD, demonstrating that present IMD FT can be effectively used as labelling agent for LFPs visualization.

ACCEPTED MANUSCRIPT

3.7. LFPs visualization and Anti-counterfeiting applications

Fig.11 depicts the LFPs visualized using IMD FT under UV 365 nm light on various non-porous surfaces, namely computer mouse, glass slide, metal scale, coin and spatula. Well – defined ridge characteristics with high sensitivity and up to level 2 features were clearly distinguished in all the substrates. Further, an examination was conducted to explore the probable utilization of the proposed IMD FT in the visualization of LFPs on porous surfaces, namely, magazine cover, aluminum foil, complex background paper, barcode and so on. (Fig.12). The clear ridge microstructures of FPs could be evidentially revealed without any background color disruption, indicating that the prepared IMD FT was considered to excellent agent for LFPs visualization.

In closer inspection, LFPs consists of many informative ridge details which were necessitates for personal identification. Generally, ridge details of LFPs are categorized into three levels. Level 1 gives the pattern data (arches, loops, whorls, and compounds) of the FPs. Whereas, level 2 depicts the minutia points such as, enclosure, delta, bifurcation, core, short ridge, bridge, island, hook, etc. And the level 3 consists of shape and location of sweat pores [44-46]. In the present work, visualized LFPs on curved surfaced soft drink can under UV 365 nm light evidentially reveals level 1 and level 2 ridge details. In addition, most neglected level 3 features such as sweat pores were also easily detected (Fig.13). These outstanding results are adequate for individualization and pivotal for scientific examinations of unique finger impression emerging from diverse surfaces. The obtained high-quality FPs imaging might be a results of good affinity between sweat contents and AIE. Generally, fresh LFPs sweat contains water (99 %) along with various chloride and phosphate (inorganic salts), amino acids, fatty acids, urea, and polypeptides (organic materials). Among them, hydrophobic amino acid residues are composed of core, polar and charged amino acids,

ACCEPTED MANUSCRIPT

which preferentially cover the surface of the molecule and are in contact with the solvent due to their ability to form hydrogen bonds. In the present case, the main adherence property may be due to the electrostatic interactions between the O atoms of the AIE and the H atoms of the amino acids present in the ridges of LFPs.

Further, we assessed the effect of colors on visualization of LFPs containing distinctive sweat contents. An appropriate method was utilized where a LFPs on the aluminum foil surface were stored in various time periods (1, 7, 15 and 30 days), without contacting anything in the middle of a deposition. Then, the aged LFPs were stained by IMD FT and photographed under 365 nm UV light (Fig.14 (a – d)). A bright and clear ridge details of FPs was revealed in 1 day. Further, even for the 30 days aged developed FPs reveals clear ridge details. This evident that the slight diminishing in recognition quality was established for the FPs after consecutive period. This study shows that the present IMD FT was active even at minimum sweat residues. This is a vital outcome with regards to scientific science since LFP evidence is frequently discovered hours or days after the event of the crime. In addition, pixel profile of small region of the developed LFP was shown in Fig.14 (e). From the pixel profile, it was clear that the IMD FT was stained exactly on the ridges.

Non-destructive strategies for gathering proof are critical in the field of legal sciences. Because of the geometry of the substrates, non-destructive visualization of LFPs on twisted surfaces remains challenging. In the present work, we have been developed FPs on non-porous curved surfaces (including Pepsi can and pen) by staining IMD FT and photographed under 365 nm UV light (Fig.15 (a & b)). Well-defined and clear FP minutia ridge details were revealed without further processing. Further, in order to demonstrate the efficiency of prepared IMD FT for the visualization of LFPs, control experiments using commercially used Fe_2O_3 powder was performed (Fig.15 (c & d)). The LFPs visualized utilizing IMD FT show

ACCEPTED MANUSCRIPT

more affluent ridge details with less background hindrance, indicating the better determination to empower clear distinguishing proof of the highlights of the LFPs.

To access stability of the IMD FTs, LFPs were visualized on glass surface maintained at various temperatures (25 to 39 ^{o}C) (Fig.16). It was evident that, the detection sensitivity gradually decreases with increased temperature, due to gradual evaporation of biogenic constituents present in LFPs. Although, the highest visibility was observed with clear ridge details even at high temperature. The obtained results signify that prepared IMD FTs are stable and are more sufficient for visualization of LFPs in different environmental conditions. Aforementioned results clearly evident that the present IMD FT was an effective tool for the visualization of LFPs on various porous and non-porous surfaces.

On the basis of the excellent AIE induced PL property of the prepared IMD FT, the dynamic luminescent images were designed on common paper by simple dip pen mode under RT for anti-counterfeiting applications (Fig.17). Under normal light, the images painted are not visible (Fig.17 (a- f)), but can be clearly sensed by touch. However, the luminescent images are able to show different patterns with cyan color emission under 365 nm light (Fig.17 (a^1-f^1)). Based on the obtained results, it was found that IMD FT opens up with a new strategy for the preparation of low-cost and simple security ink for anti-counterfeiting applications.

ACCEPTED MANUSCRIPT

ACCEPTED MANUSCRIPT

4. Conclusions

In summary, herein a new simple and inexpensive IMD FTs were prepared via simple acid catalyzed five-member N-heterocyclic ring forming reaction process, which exhibits an attractive AIE feature in both mixed aqueous media and solid state. It does not require complex instrumentation, pre or post handling of the processed special storage environments. Superior hydrophobic interaction between these IMD FT and LFPs content was strategically used to improve and visualize the LFPs on any versatile surfaces. The visualized LFPs reveals level I to level III ridge features with high efficiency, selectivity, low contrast and without any background hindrance. The IMD FTs with a suitable PVC medium offers the superior resolution and transparent security ink. These results indicated that the AIE based IMD FT was considered to be promising candidate for LFPs visualization and anti-counterfeiting applications.

Acknowledgement

The author Dr. H Nagabhushana thanks to VGST, Govt. of Karnataka, India [VGST/KFIST-4/GRD-489] for the sanction of this project.

ACCEPTED MANUSCRIPT

ACCEPTED MANUSCRIPT

References

[1] Xiaodong Jin, Ran Xin, Shifan Wang, Wenzhu Yin, Tongxiang Xu, Yang Jiang, Xuran Ji, Luyang Chen, Jingning Liu, A tetraphenylethene-based dye for latent fingerprint analysis, Sens. Actuators B, 244 (2017) 777–784.

[2] Walid M. Abdelwahab, Edjohnier Phillips, Gabor Patonay, Preparation of fluorescently labeled silica nanoparticles using an amino acid-catalyzed seeds regrowth technique: Application to latent fingerprints detection and hemocompatibility studies, J. Colloid Int. Sci., 512 (2018) 801-811.

[3] Maude Desroches, Jean-François Morin, Anthanthrene as a super-extended tetraphenylethylene for aggregation-induced emission, Org. Lett., 20 (2018) 2797-2801.

[4] Kirti Kumari Sharma, Peethani Nagaraju, Maneesha Esther Mohanty, Tulsidas Ramchandar Rao Baggi, Vaidya Jayathirtha Rao, Latent fingermark development using a novel phenanthro imidazole derivative, J. Photochem. Photobiol. A, 351 (2018) 253-260.

[5] Gereon A. Sommer, Larisa N. Mataranga-Popa, Rafal Czerwieniec, Thomas Hofbeck, Herbert H. H. Homeier, Thomas J.J. Müller, Hartmut Yersin, Design of conformationally distorted donor–acceptor dyads showing efficient thermally activated delayed fluorescence, J. Phys. Chem. Lett., 9 (2018) 3692-3697.

[6] Jianjun Du, Jiangli Fan, Xiaojun Peng, Honglin Li, Shiguo Sun, The quinoline derivative of ratiometric and sensitive fluorescent zinc probe based on deprotonation, Sens. Actuators B, 144 (2010) 337-341.

[7] S. Xue, X. Qiu, Q. Sun, W. Yang, Alkyl length effects on solid-state fluorescence and mechanochromic behavior of small organic luminophores, J. Mater. Chem. C, 4 (2016) 1568-78.

[8] G.P. Darshan, H.B. Premkumar, H. Nagabhushana, S.C. Sharma, B. Daruka Prasad, S.C. Prashantha, R.B. Basavaraj, Superstructures of doped yttrium aluminates for luminescent and advanced forensic investigations, J. Alloys Compd., 686 (2016) 577 – 587.

[9] R.B. Basavaraj, H. Nagabhushana, G.P. Darshan, B. Daruka Prasad, S.C. Sharma, K.N. Venkatachalaiah, Ultrasound assisted rare earth doped Wollastonite nanopowders: Labeling agent for imaging eccrine latent fingerprints and cheiloscopy applications, J. Ind. Eng. Chem., 51 (2017) 90-105.

ACCEPTED MANUSCRIPT

[10] M. Dhanalakshmi, H. Nagabhushana, R.B. Basavaraj, G. P. Darshan, B. Daruka Prasad, Surfactant-assisted $BaTiO_3:Eu^{3+}@SiO_2$ core–shell superstructures obtained by ultrasonication method: Dormant fingerprint visualization and red component of white light-emitting diode applications, ACS Sustainable Chem. Eng., 6 (2018) 5214-5226.

[11] A. Sandhyarani, M.K. Kokila, G.P. Darshan, R.B. Basavaraj, B. Daruka Prasad, S.C. Sharma, T.K.S. Lakshmi, H. Nagabhushana, Versatile core-shell $SiO_2@SrTiO_3:Eu^{3+}$, Li^+ nanopowders as fluorescent label for the visualization of latent fingerprints and anti-counterfeiting applications, Chem. Eng. J., 327 (2017) 1135-1150.

[12] Joosub Lee, Minkyeong Pyo, Sang-hwa Lee, Jaeyong Kim, Moonsoo Ra, Whoi-Yul Kim, Bum Jun Park, Chan Woo Lee, Jong-Man Kim, Hydrochromic conjugated polymers for human sweat pore mapping, Nature comm., 5 (2014) 3736-3746.

[13] N.H. Deepthi, G.P. Darshan, R.B. Basavaraj, B. Daruka Prasad, H. Nagabhushana, Large-scale controlled bio-inspired fabrication of 3D $CeO_2:Eu^{3+}$ hierarchical structures for evaluation of highly sensitive visualization of latent fingerprints, Sens. Actuators B, 255 (2018) 3127-3147.

[14] Raghupathy Suresh, Senthil Kumar Thiyagarajan, Perumal Ramamurthy, An AIE based fluorescent probe for digital lifting of latent fingerprint marks down to minutiae level, Sens. Actuators B, 258 (2018) 184–192.

[15] G.P. Darshan, H.B. Premkumar, H. Nagabhushana, S.C. Sharma, S.C. Prashanth, B. Daruka Prasad, Effective fingerprint recognition technique using doped yttrium aluminate nanophosphor material, J. Coll. Inter. Sci., 464 (2016) 206-218.

[16] Y. Li, L. Xu, B. Su, Aggregation induced emission for the recognition of latent fingerprints, Chem. Commun., 34 (2012) 4109–4111.

[17] X.D. Jin, L.B. Dong, X.Y. Di, H. Huang, J.N. Liu, X.L. Sun, X.Q. Zhang, H.J. Zhu, NIR luminescence for the detection of latent fingerprints based on ESIPT and AIE processes, RSC Adv., 5 (2015) 87306–87310.

[18] X.D. Jin, R. Xin, S.F. Wang, W.Z. Yin, T.X. Xua, Y. Jiang, X.R. Ji, L.Y. Chen, J.N. Liu, A tetraphenylethene-based dye for latent fingerprint analysis, Sens. Actuators B, 244 (2017) 777–784.

[19] J.D. Luo, Z.L. Xie, J.W.Y. Lam, L. Cheng, H.Y. Chen, C.F. Qiu, H.S. Kwok, X.W. Zhan, Y.Q. Liu, D.B. Zhu, B.Z. Tang, Aggregation-induced emission of 1-methyl-1,2,3,4,5-pentaphenylsilole, Chem. Commun., 174 (2001) 1740–1741.

[20] G.P. Darshan, H.B. Premkumar, H. Nagabhushana, S.C. Sharma, B. Daruka Prasad, S.C. Prashantha Neodymium doped yttrium aluminate synthesis and optical properties - A

ACCEPTED MANUSCRIPT

blue light emitting nanophosphor and its use in advanced forensic analysis, Dyes Pigm., 134 (2016) 227-233.

[21] Xiaodong Jin, Ran Xin, Shifan Wang, Wenzhu Yin, Tongxiang Xu, Yang Jiang, Xuran Ji, Luyang Chen, Jingning Liu, A tetraphenylethene-based dye for latent fingerprint analysis, Sens. Actuators B, 244 (2017) 777-784.

[22] Rui Liu, Zhongming Song, Yuhao Li, Yang Li, Wanwan Yao, Haoling Sun, Hongjun Zhu, An AIPE-active heteroleptic Ir(III) complex for latent fingermarks detection, Sens. Actuators B, 259 (2018) 840–846.

[23] Joosub Lee, Minkyeong Pyo, Sang-hwa Lee, Jaeyong Kim, Moonsoo Ra, Whoi-Yul Kim, Bum Jun Park, Chan Woo Lee, Jong-Man Kim, Hydrochromic conjugated polymers for human sweat pore mapping, Nature comm., 5 (2014) 3736-3746.

[24] J. Kai, L. Zhang, J. Lu, C. Xu, C. Cai, H. Lin, Triple-mode emission of carbon dots: applications for advanced anti-counterfeiting, Angew. Chem., 55 (2016) 1–6.

[25] G.P. Darshan, H.B. Premkumar, H. Nagabhushana, S.C. Sharma, S.C. Prashantha, H.P. Nagaswarupa, B. Daruka Prasad, Blue light emitting ceramic nano-pigments of Tm^{3+} doped $YAlO_3$: Applications in latent finger print, anti-counterfeiting and porcelain stoneware, Dyes Pigm., 131 (2016) 268-281.

[26] B. Marappa, M.S. Rudresha, R.B. Basavaraj, G.P. Darshan, B. Daruka Prasad, S.C. Sharma, S. Sivakumari, P. Amudha, H. Nagabhushana, EGCG assisted $Y_2O_3:Eu^{3+}$ nanopowders with 3D micro-architecture assemblies useful for latent finger print recognition and anti-counterfeiting applications, Sens. Actuators B, 264 (2018) 426-439.

[27] J. Wang, C.F. Wang, S. Chen, Amphiphilic egg-derived carbon dots: rapid plasma fabrication, pyrolysis process, and multicolor printing patterns, Angew. Chem., Int. Ed. 51 (2012) 9297-9301.

[28] F. Li, X. Wang, Z. Xia, C. Pan, Q. Liu, Photoluminescence tuning in stretchable PDMS film grafted doped core/multishell quantum dots for anti-counterfeiting, Adv. Fun. Mater., 27 (2017) 1700051.

[29] G.P. Darshan, H.B. Premkumar, H. Nagabhushana, S.C. Sharma, B. Umesh, R.B. Basavaraj, Nucleation and self-assembly dynamics of hierarchical $YAlO_3:Ce^{3+}$ architectures: Nano probe for in vitro dermatoglyphics and anti-mimetic applications, Mat. Sci. & Eng. C, 99 (2019) 282-295.

[30] C.D. Tran, Y. Cui, S. Smirnov, Simultaneous multispectral imaging in the visible and near infrared region: applications in document authentication and determination of chemical inhomogeneity of copolymers, Anal. Chem., 70 (1998) 4701-4708.

ACCEPTED MANUSCRIPT

[31] F. Femila Komahal, H. Nagabhushana, R.B. Basavaraj, G.P. Darshan, B. Daruka Prasad, S.C. Sharma, D. Kavyashree, Design of Bi-functional composite core–shell SiO_2@$ZnAl_2O_4$:Eu^{3+} array as a fluorescent sensor for selective and sensitive latent fingerprints visualization protocol, Adv. Powder Tech. 29 (2018) 1991-2002.

[32] Kai Li, Xi Su, Yixuan Wang, Furong Tao, Yuezhi Cui, Huayong Zhang, Tianduo Li, D-π-A type barbituric derivatives: Aggregation induced emission, mechanofluorochromic and solvatochromic properties, J. Lumin., 203 (2018) 50–58.

[33] B. Hemavathi, C. Trupthi Devaiah, M.G. Swathi, T.N. Ahipa, Influence of terminal alkoxy chain lengths on the solvatochromic and AIE properties of 4,6-bis(4-(3,4-bis(alkoxy)styryl)phenyl)-2-methoxynicotinonitriles, Dyes Pigm., 159 (2018) 1–7.

[34] M.G. Swathi, T.N. Ahipa, Aggregation induced emission properties of new cyanopyridone derivatives, J. Mol. Liq., 265 (2018) 747–755.

[35] Hui Li, Yang Guo, Guoxing Li, Hongping Xiao, Yunxiang Lei, Xiaobo Huang, Jiuxi Chen, Huayue Wu, Jinchang Ding, Yixiang Cheng, Aggregation-induced fluorescence emission properties of Dicyanomethylene-1,4-dihydropyridine derivatives, J. Phys. Chem. C, 119 (2015) 6737–6748.

[36] Jie Zheng, Fang Huang, Yujin Li, Tianwei Xu, Hui Xu, Jianhong Jia, Qing Ye, Jianrong Gao, The aggregation-induced emission enhancement properties of BF_2 complex isatin-phenylhydrazone: Synthesis and fluorescence characteristics, Dyes Pigm., 113 (2015) 502-509.

[37] Junhui Jia, Huijuan Zhang, Mechanofluorochromic properties of tert-butylcarbazole-based AIE-active D-π-A fluorescent dye, J. Photochem. Photobiol. A, 353 (2018) 521-526.

[38] Huaizhi Gao, Defang Xu, Yonghui Wang, Chao Zhang, Yan Yang, Xingliang Liu, Aixia Han, Ying Wang, Aggregation-induced emission and mechanofluorochromism of tetraphenylbutadiene modified β-ketoiminate boron complexes, Dyes Pigm., 150 (2018) 165–173.

[39] C. Suresh, H. Nagabhushana, R.B. Basavaraj, G.P. Darshan, D. Kavyashree, B. Daruka Prasad, S.C. Sharma, R. Vanithamani, SiO_2@LaOF:Eu^{3+} core-shell functional nanomaterials for sensitive visualization of latent fingerprints and WLED applications, J. Colloid Interface Sci., 518 (2018) 200-215.

[40] Xiaobo Huang, Lebin Qian, Yibin Zhou, Miaochang Liu, Yixiang Cheng, Huayue Wu, Effective structural modification of traditional fluorophores to obtain organic mechanofluorochromic molecules, J. Mater. Chem. C, 6 (2018) 5075-5096.

ACCEPTED MANUSCRIPT

[41] Fei Zhao, Zhao Chen, Gang Liu, Congbin Fan, Shouzhi Pu, Tetraphenylethene-based highly emissive fluorescent molecules with aggregation-induced emission (AIE) and various mechanofluorochromic characteristics, Tetrahedron Lett., 59 (2018) 836-840.

[42] Yuyang Zhang, Yuqing Ma, Lin Kong, Yupeng Tian, Jiaxiang Yang, A novel indolo [3,2-b]carbazole derivative with D-π-A structure exhibiting aggregation-enhanced emission and mechanofluorochromic properties, Dyes Pigm., 159 (2018) 314-321.

[43] Yonghui Wang, Defang Xu, Huaizhi Gao, Ying Wang, Xingliang Liu, Aixia Han, Chao Zhang, Ling Zang, Mechanofluorochromic properties of aggregation-induced emission-active tetraphenylethene-containing cruciform luminophores, Dyes Pigm., 156 (2018) 291-298.

[44] L. Deininger, S. Francese, M.R. Clench, G. Langenburg, V. Sears, C. Sammon, Investigation of infinite focus microscopy for the determination of the association of blood with fingermarks, Sci. & Justice, https://doi.org/10.1016/j.scijus.2018.07.001.

[45] H.S. Yogananda, R.B. Basavaraj, G.P. Darshan, B. Daruka Prasad, Ramachandra Naik, S.C. Sharma, H. Nagabhushana, New design of highly sensitive and selective $MoO_3:Eu^{3+}$ micro-rods: Probing of latent fingerprints visualization and anti-counterfeiting applications, J. Colloid Int. Sci., 528 (2018) 443-456.

[46] K.N. Venkatachalaiah, H. Nagabhushana, G.P. Darshan, R.B. Basavaraj, B. Daruka Prasad, Novel and highly efficient red luminescent sensor based $SiO_2@Y_2O_3:Eu^{3+}$, M^+ (M^+=Li, Na, K) composite core–shell fluorescent markers for latent fingerprint recognition, security ink and solid state lightning applications, Sens. Actuators B, 251 (2017) 310-325.

ACCEPTED MANUSCRIPT

ACCEPTED MANUSCRIPT

ACCEPTED MANUSCRIPT

Table 1: Crystal data and structure refinement of IMD FT

Compound	**IMD (4)**
Empirical formula	$C_{29}H_{18}F_6N_2O$
Formula weight	524.45
Temperature	150(2) K
Wavelength	0.71073 Å
Crystal system, space group	Triclinic
Unit cell dimensions	
a (Å)	8.6744(9)
b (Å)	11.3188(14)
c (Å)	12.8607(15)
α (°)	68.496(4)°
β (°)	β= 81.524(4)°
γ (°)	γ = 75.144(4)°
Volume ($Å^3$)	1133.5(2)
Z	2
Density (calculated)	1.537 Mg/m^3
Absorption coefficient	0.128 mm^{-1}
F(000)	536
Crystal size	0.480 x 0.270 x 0.250 mm^3
Theta range for data collection	2.781 to 26.366°.
Index ranges	-9<=h<=10, -14<=k<=14, -16<=l<=16
Reflections collected	19346
Independent reflections	4425 [R(int) = 0.0543]
Completeness to theta = 25.242°	96.0 %
Absorption correction	Semi-empirical from equivalents
Max. and min. transmission	0.9281 and 0.8249
Refinement method	Full-matrix least-squares on F^2
Data / restraints / parameters	4425 / 0 / 347
Goodness-of-fit on F^2	1.273
Final R indices [I>2sigma(I)]	R1 = 0.0580, wR2 = 0.1660
R indices (all data)	R1 = 0.0845, wR2 = 0.1861
Extinction coefficient	n/a
Largest diff. peak and hole	0.285 and -0.367 $e.Å^{-3}$

ACCEPTED MANUSCRIPT

ACCEPTED MANUSCRIPT

Research highlights

1. A novel aggregation induced blue light emitting IMD fluorescent tag was prepared by simple route.
2. Mechanofluorochromic and Lipophicity properties of the samples were extensively studied.
3. The prepared IMD FT can be explored as a fluorescent labelling agent for the visualization of unique sweat pores on various surfaces.
4. The optimized product is highly useful in OLEDs, advanced forensic science and anti-counterfeiting applications.

ACCEPTED MANUSCRIPT

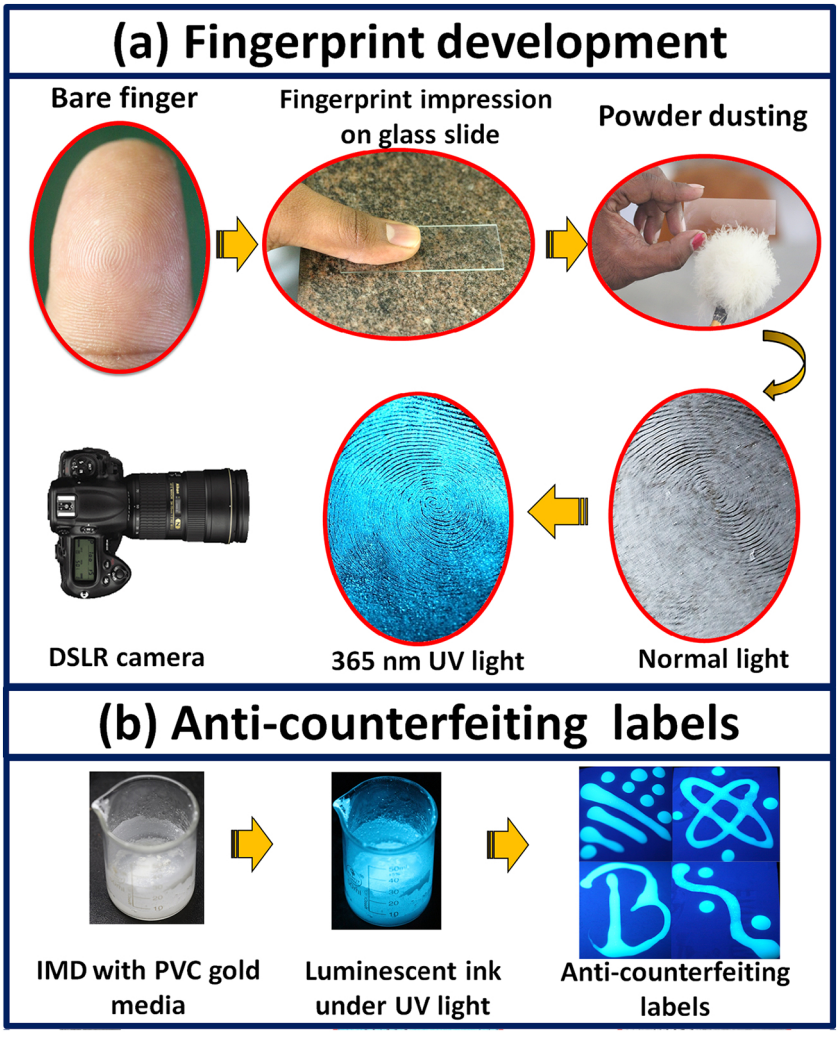
(a) Fingerprint development
Bare finger
Fingerprint impression on glass slide
Powder dusting
DSLR camera
365 nm UV light
Normal light
(b) Anti-counterfeiting labels
IMD with PVC gold media
Luminescent ink under UV light
Anti-counterfeiting labels

Figure 1

Scheme-1: Synthesis of 2-(1-(3,5-bis(trifluoromethyl)phenyl)-4,5-diphenyl-*1H*-imidazol-2-yl)phenol (4)

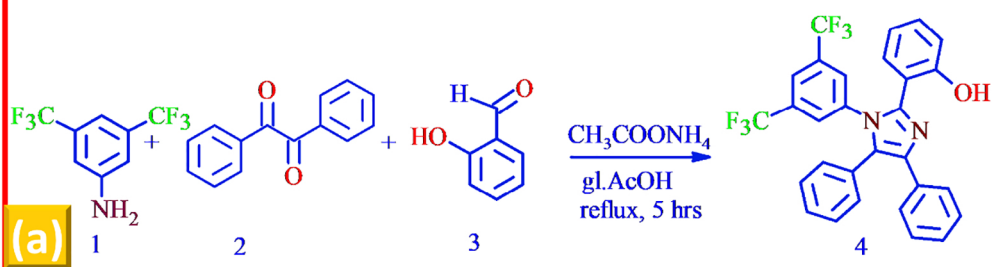

(a)

Mechanism:Synthesis of 2-(1-(3,5-bis(trifluoromethyl)phenyl)-4,5-diphenyl-*1H*-imidazol-2-yl)phenol (4)

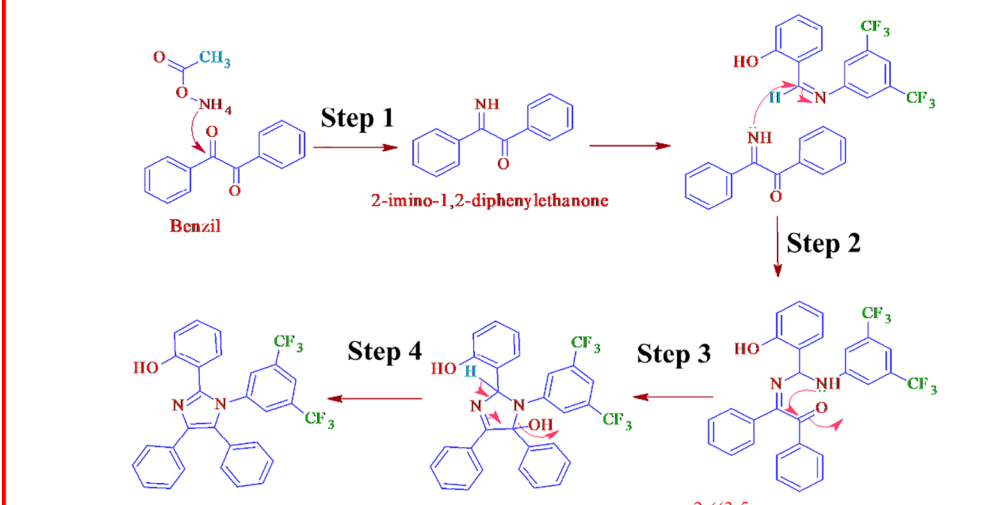

(b)

Figure 2

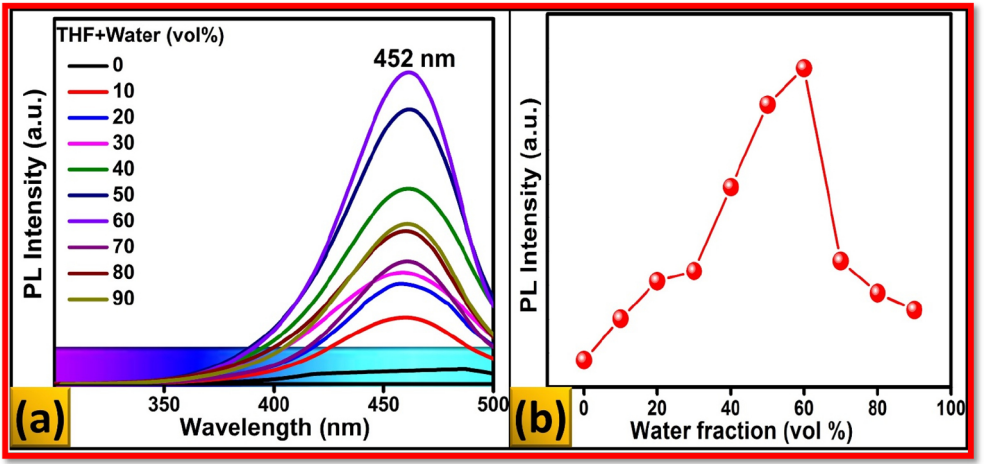
THF+Water (vol%)
0
10
20
30
40
50
60
70
80
90
452 nm
PL Intensity (a.u.)
350
400
450
500
Wavelength (nm)
(a)
PL Intensity (a.u.)
0
20
40
60
80
100
Water fraction (vol %)
(b)

Figure 3

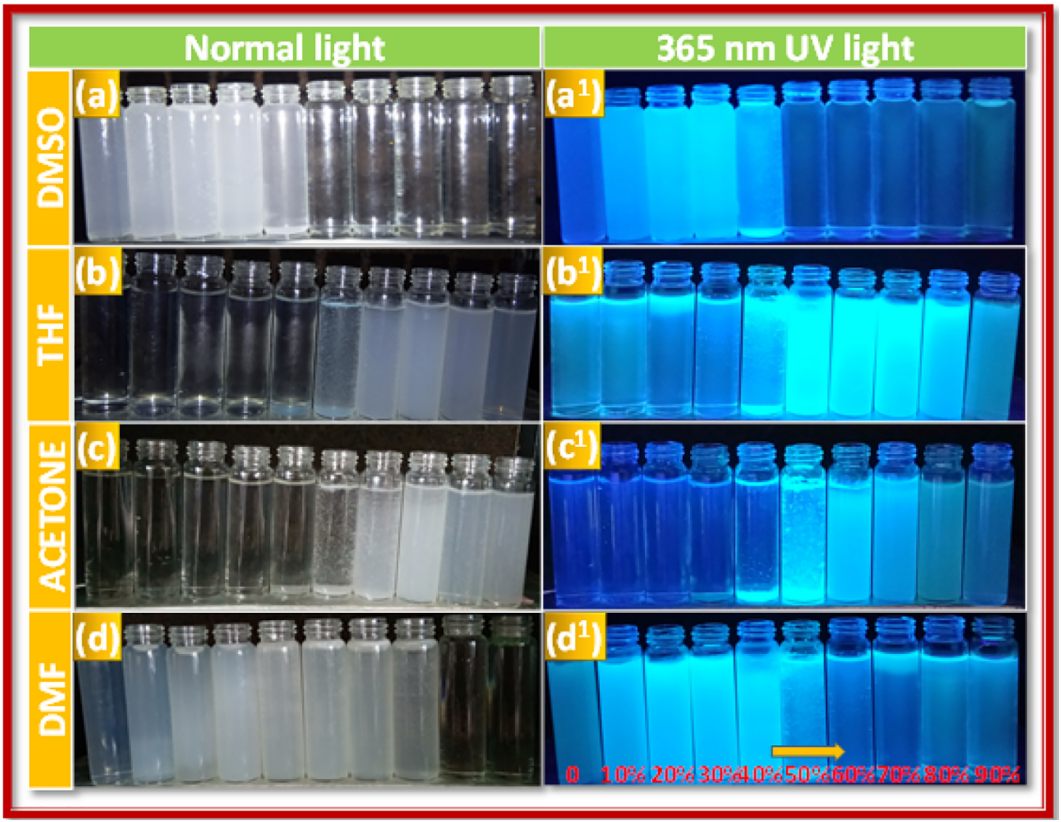
Normal light
365 nm UV light
DMSO
THF
ACETONE
DMF
(a)
(a1)
(b)
(b1)
(c)
(c1)
(d)
(d1)
0 10% 20% 30% 40% 50% 60% 70% 80% 90%

Figure 4

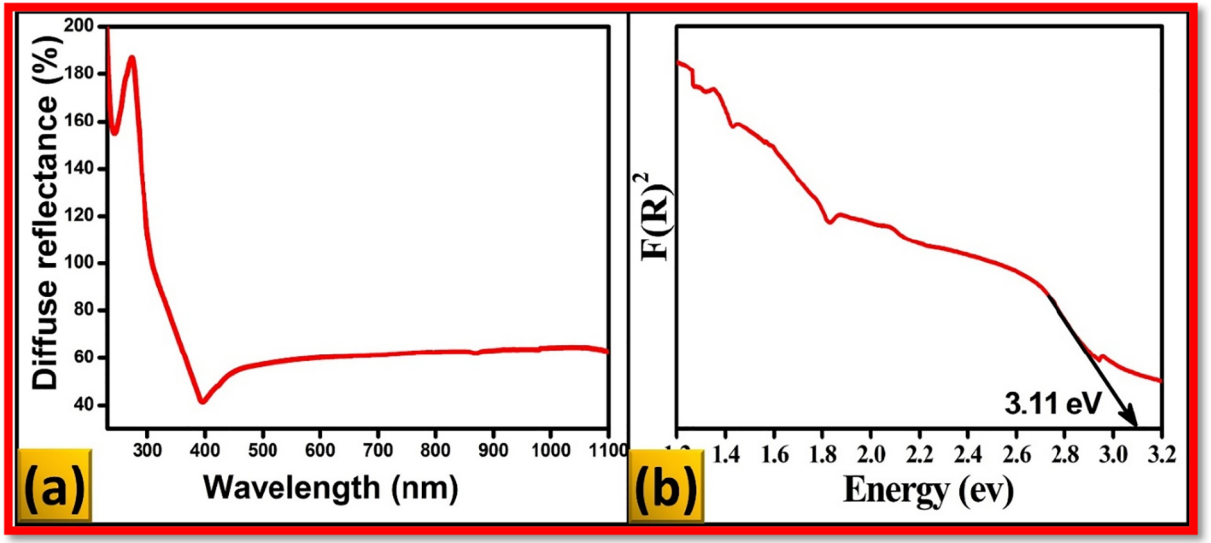
Diffuse reflectance (%)
200
180
160
140
120
100
80
60
40
300
400
500
600
700
800
900
1000
1100
Wavelength (nm)
(a)
F(R)2
3.11 eV
1.4
1.6
1.8
2.0
2.2
2.4
2.6
2.8
3.0
3.2
Energy (ev)
(b)

Figure 5

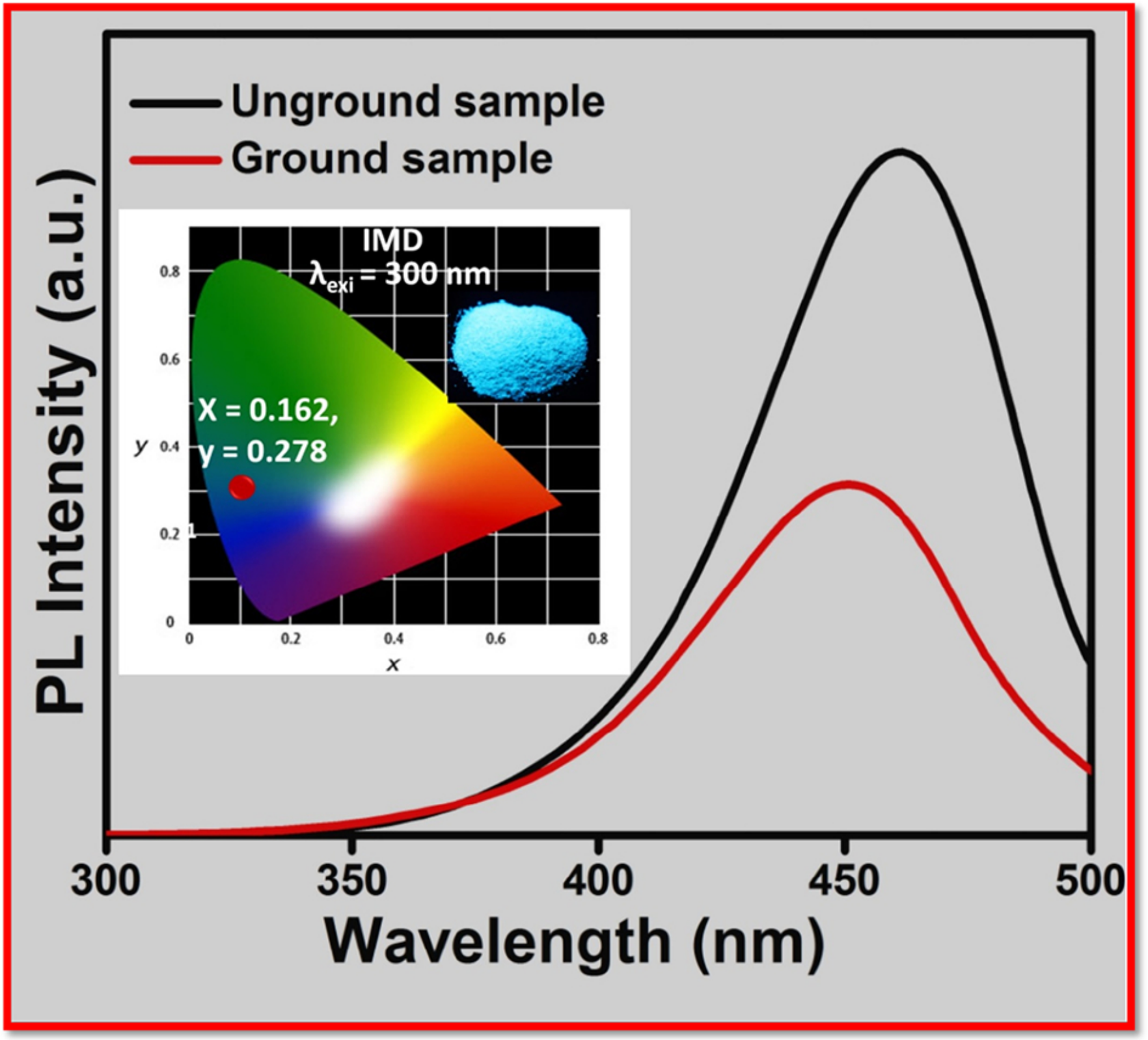
Unground sample
Ground sample
PL Intensity (a.u.)
IMD
λ_{exi} = 300 nm
X = 0.162,
y = 0.278
y
x
0
0.2
0.4
0.6
0.8
300
350
400
450
500
Wavelength (nm)

Figure 6

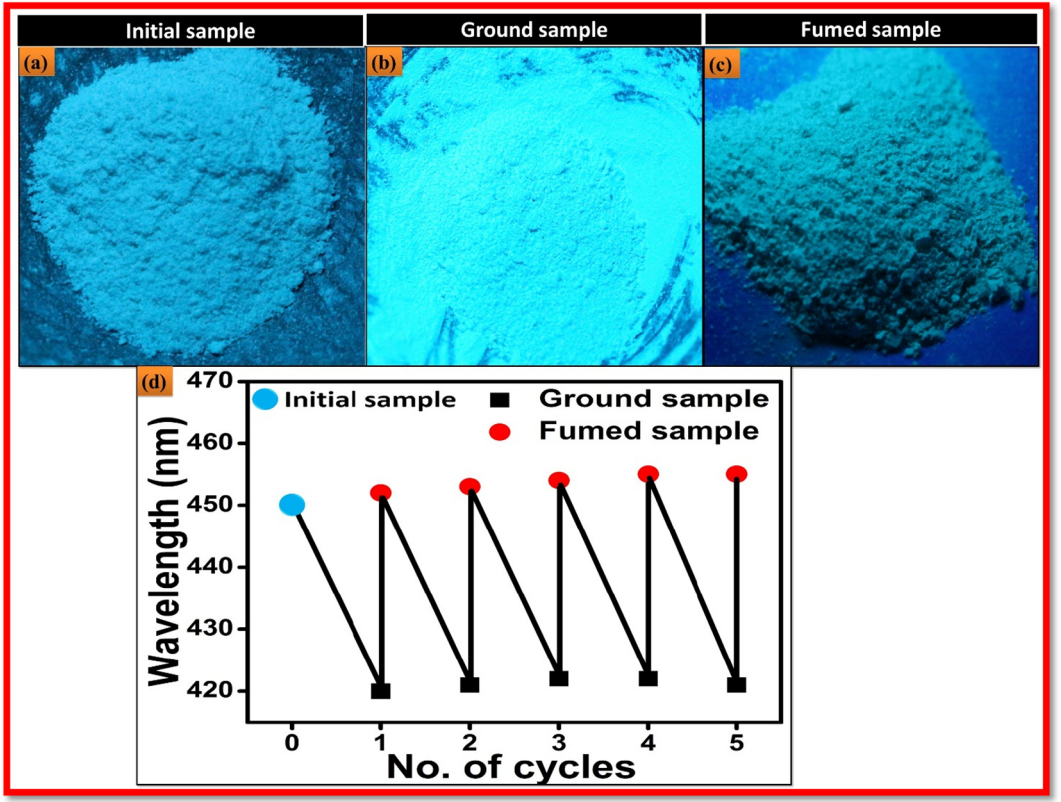
Initial sample
Ground sample
Fumed sample
(a)
(b)
(c)
(d)
Initial sample
Ground sample
Fumed sample
Wavelength (nm)
470
460
450
440
430
420
0
1
2
3
4
5
No. of cycles

Figure 7

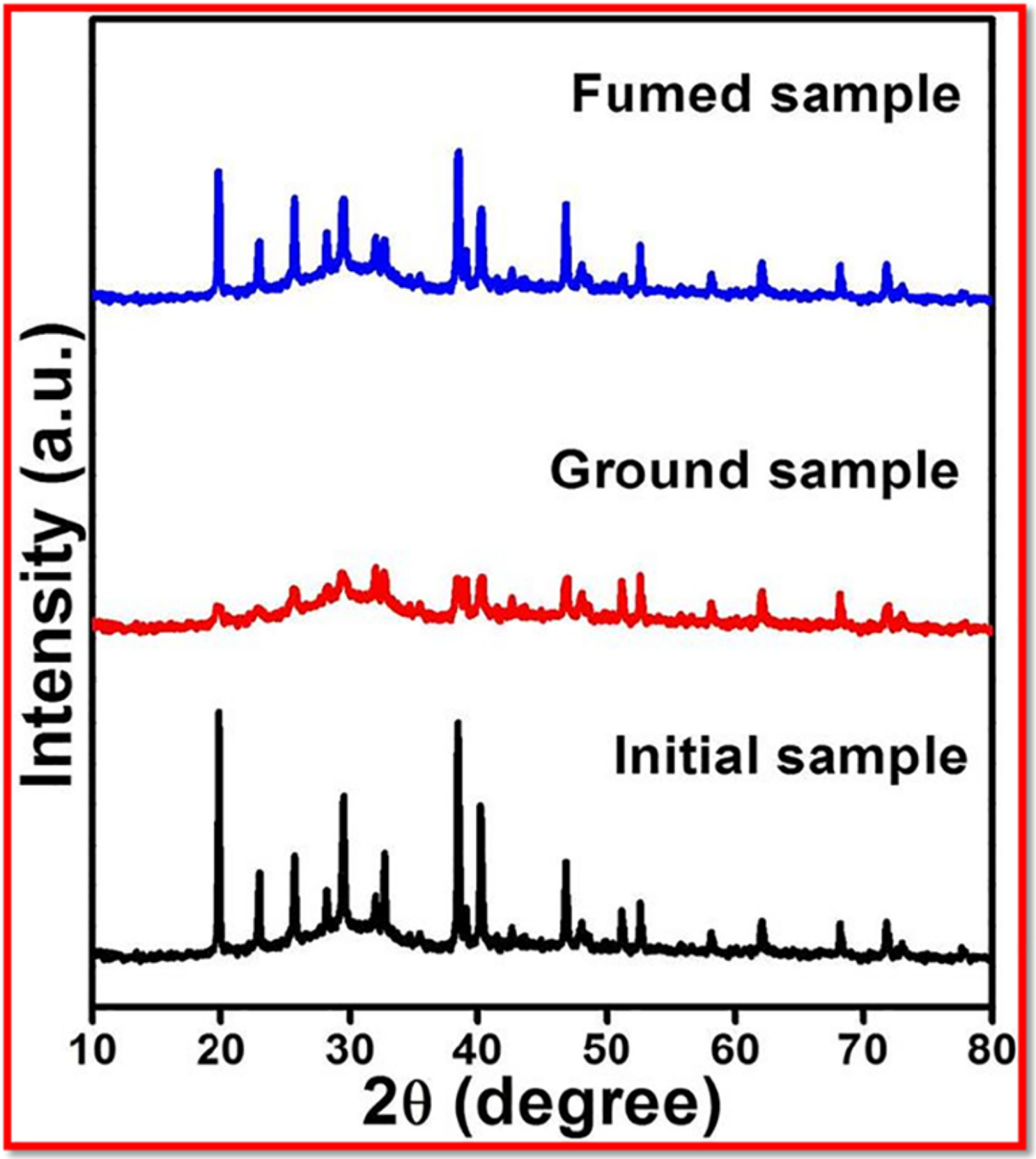
Fumed sample
Ground sample
Initial sample
Intensity (a.u.)
10
20
30
40
50
60
70
80
2θ (degree)

Figure 8

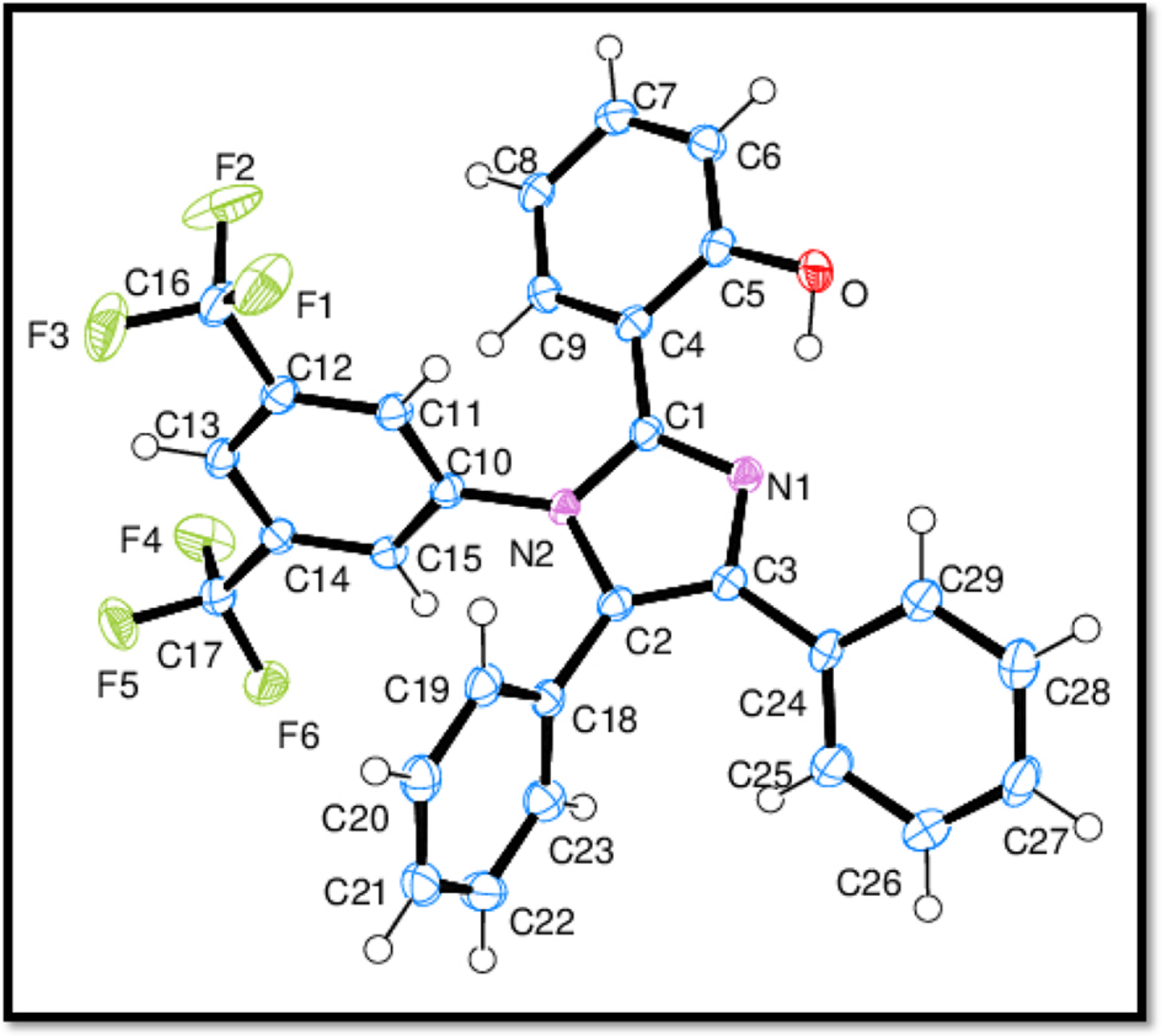
C7
C8
C6
F2
C16
F1
F3
C5
O
C9
C4
C12
C11
C1
C13
C10
N1
F4
C14
C15
N2
C3
C29
C2
F5
C17
C19
C18
C24
C28
F6
C25
C20
C23
C27
C21
C22
C26

Figure 9

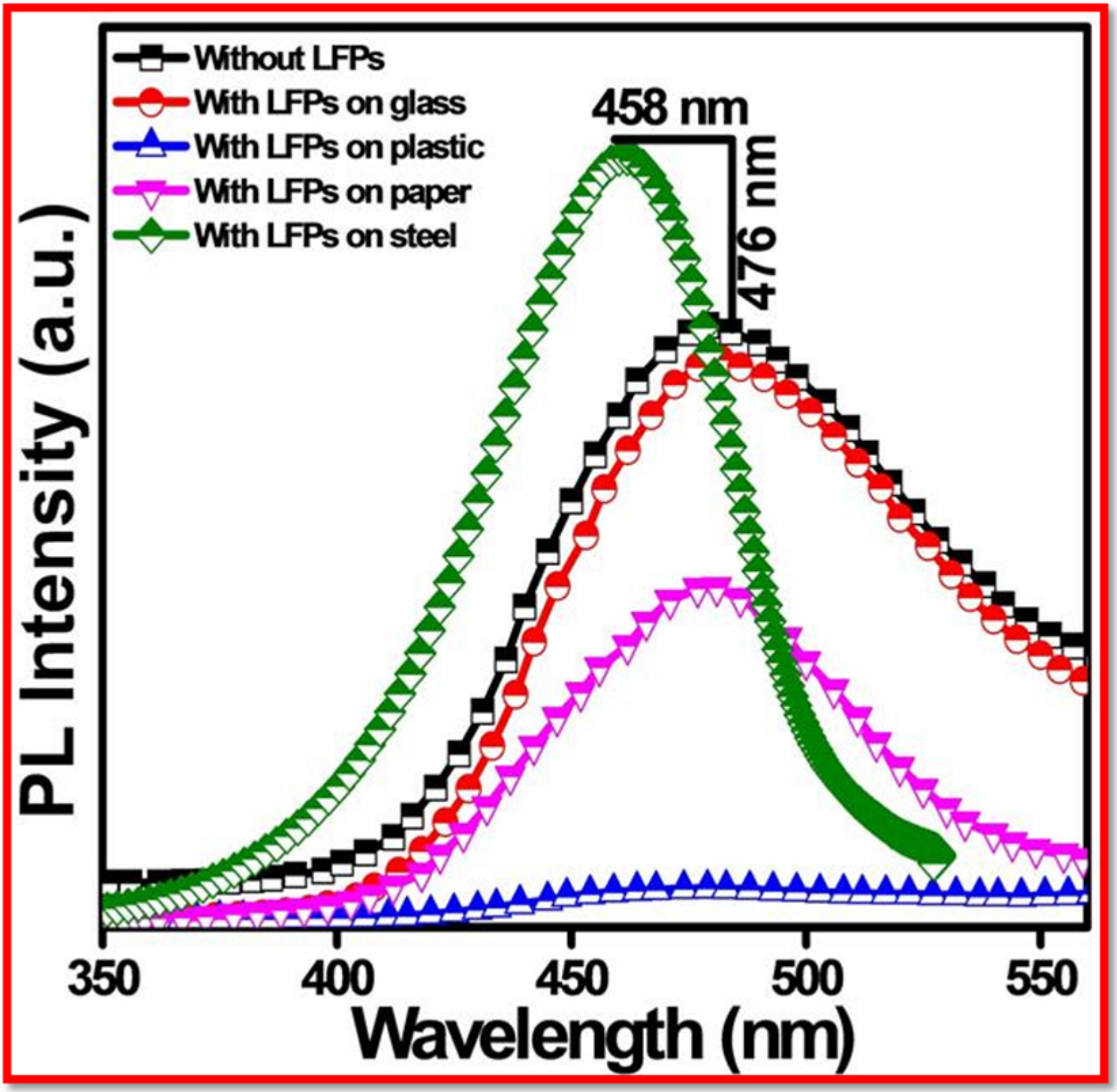
Without LFPs
With LFPs on glass
With LFPs on plastic
With LFPs on paper
With LFPs on steel
458 nm
476 nm
PL Intensity (a.u.)
350
400
450
500
550
Wavelength (nm)

Figure 10

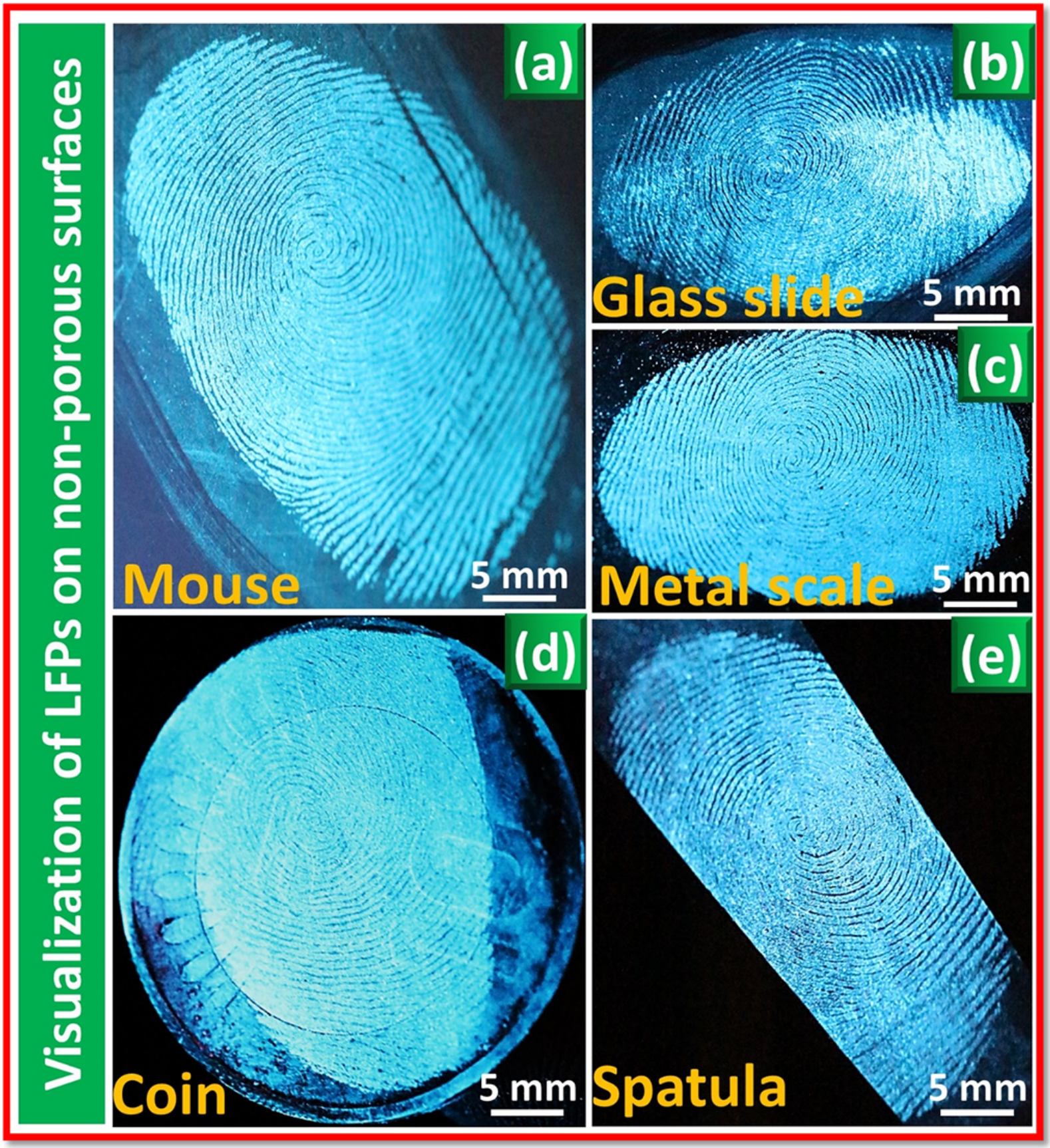
Visualization of LFPs on non-porous surfaces
(a)
Mouse
5 mm
(b)
Glass slide
5 mm
(c)
Metal scale
5 mm
(d)
Coin
5 mm
(e)
Spatula
5 mm

Figure 11

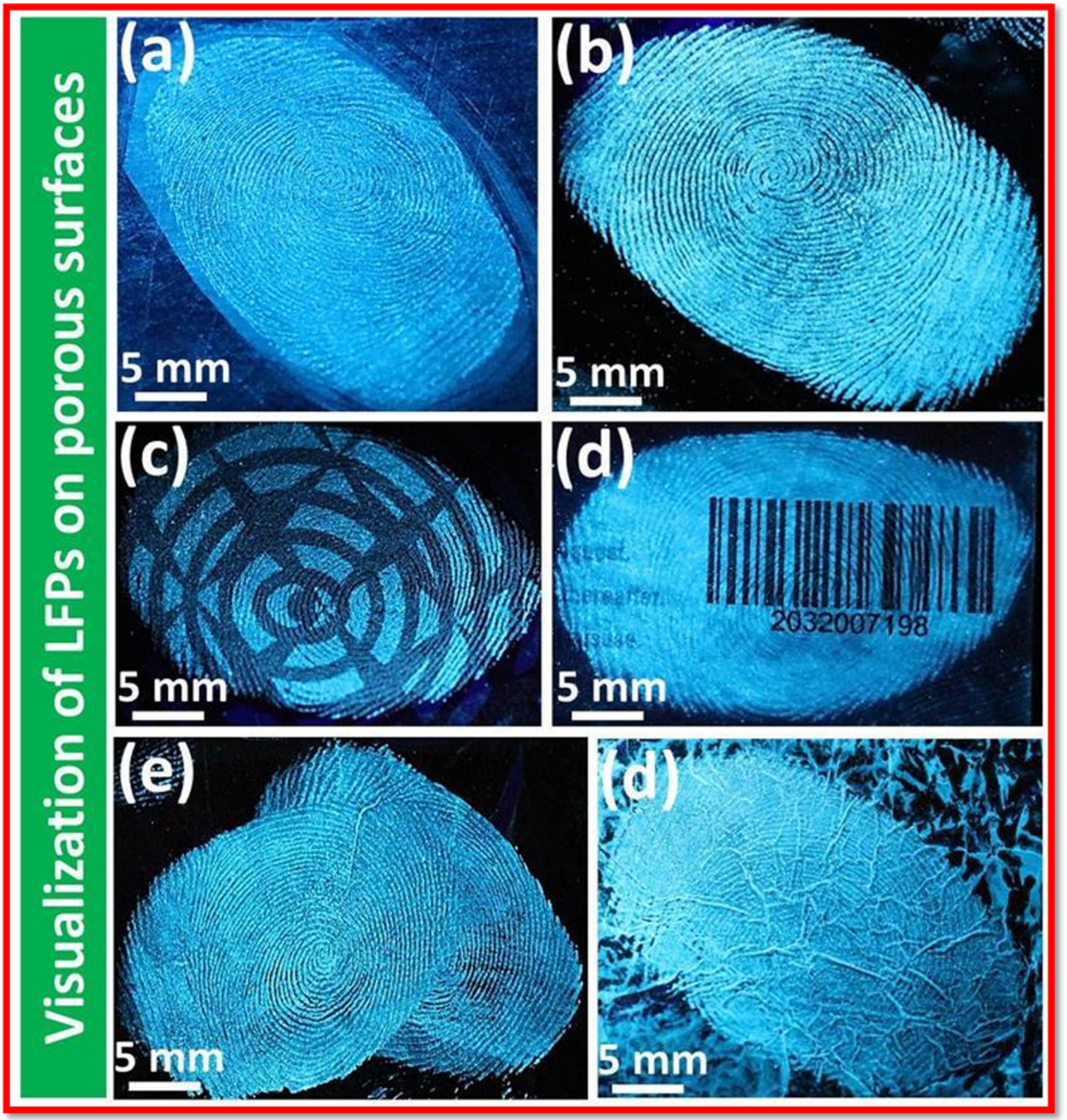
Visualization of LFPs on porous surfaces
(a)
5 mm
(b)
5 mm
(c)
5 mm
(d)
2032007198
5 mm
(e)
5 mm
(d)
5 mm

Figure 12

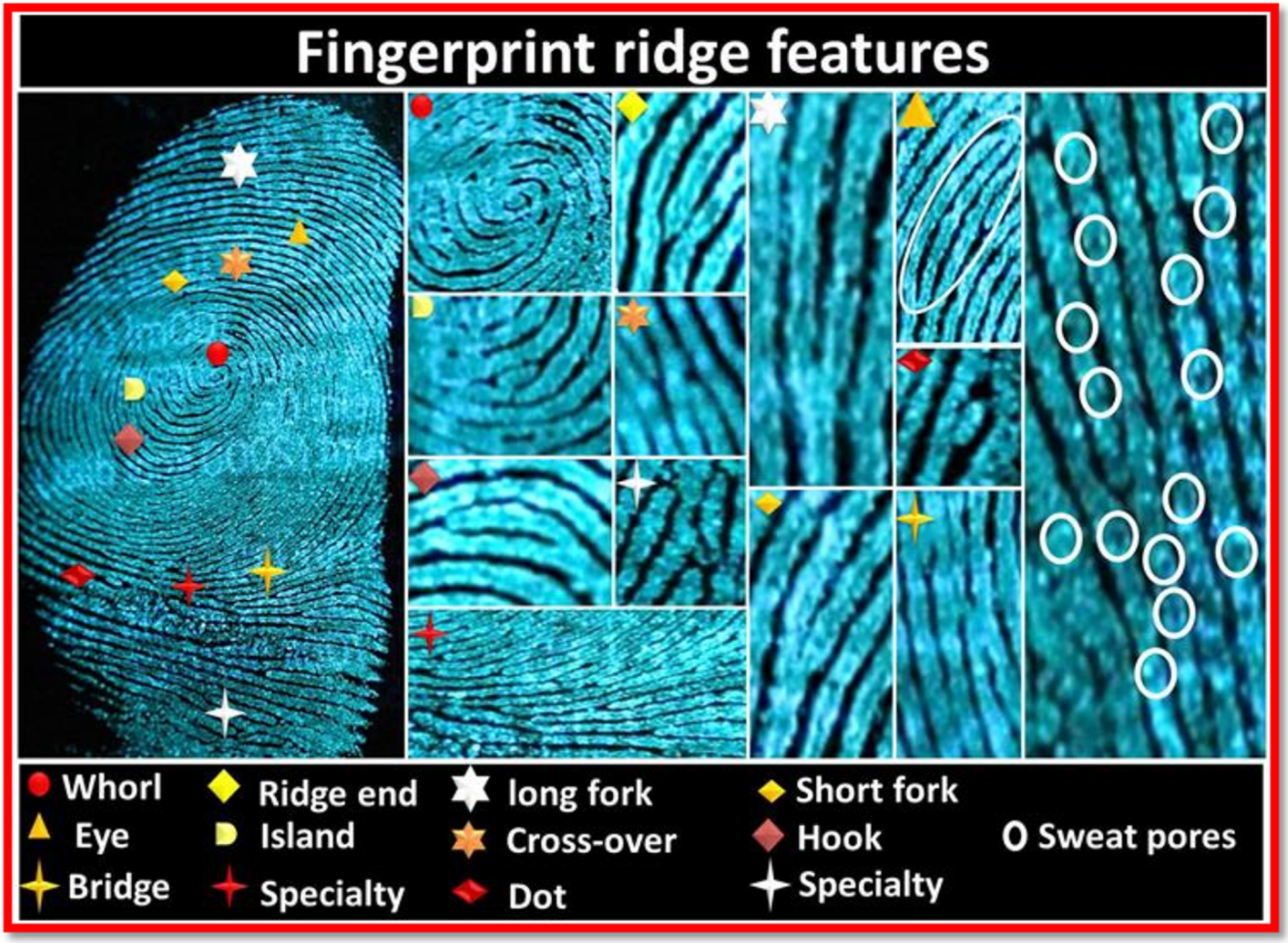
Fingerprint ridge features
Whorl
Ridge end
long fork
Short fork
Eye
Island
Cross-over
Hook
Sweat pores
Bridge
Specialty
Dot
Specialty

Figure 13

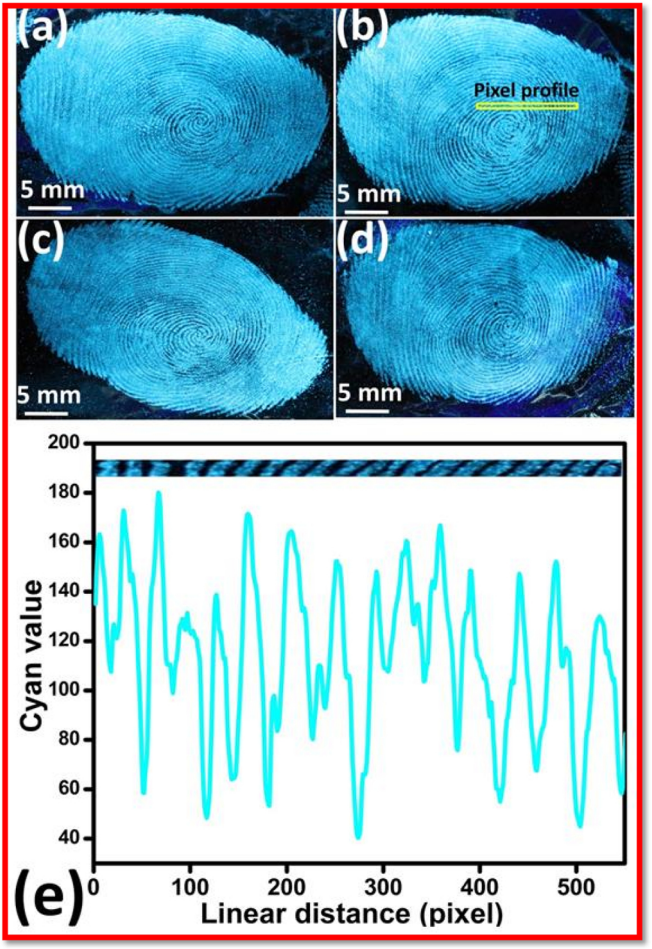
(a)
5 mm
(b)
Pixel profile
5 mm
(c)
5 mm
(d)
5 mm
(e)
Cyan value
200
180
160
140
120
100
80
60
40
0
100
200
300
400
500
Linear distance (pixel)

Figure 14

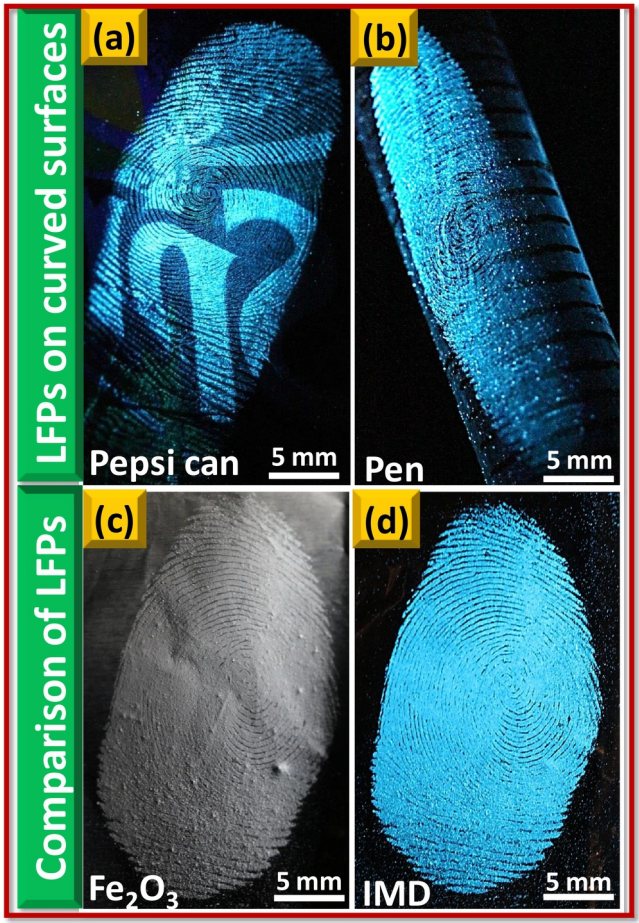
LFPs on curved surfaces
(a)
Pepsi can
5 mm
(b)
Pen
5 mm
Comparison of LFPs
(c)
Fe_2O_3
5 mm
(d)
IMD
5 mm

Figure 15

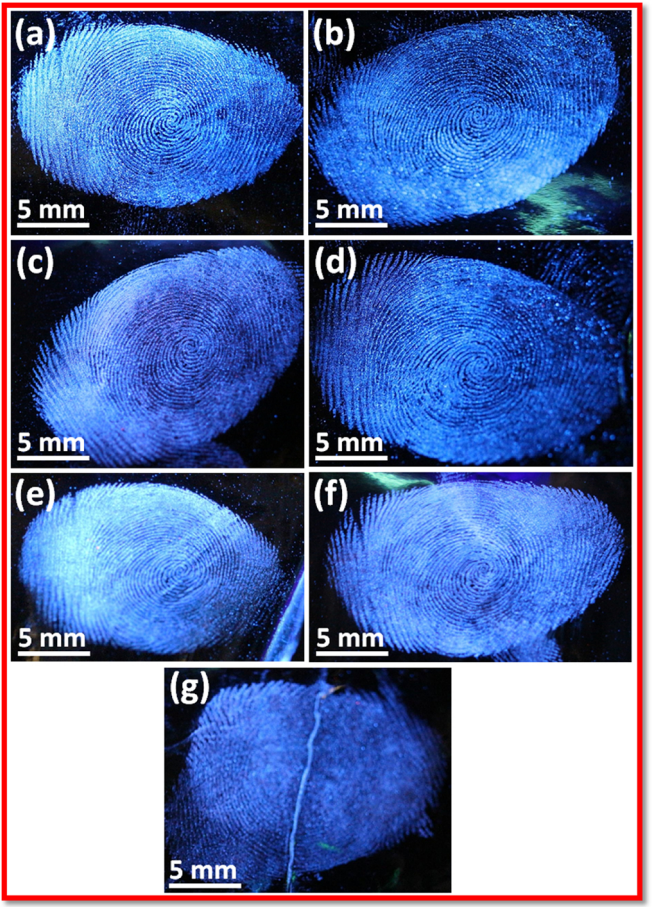

Figure 16

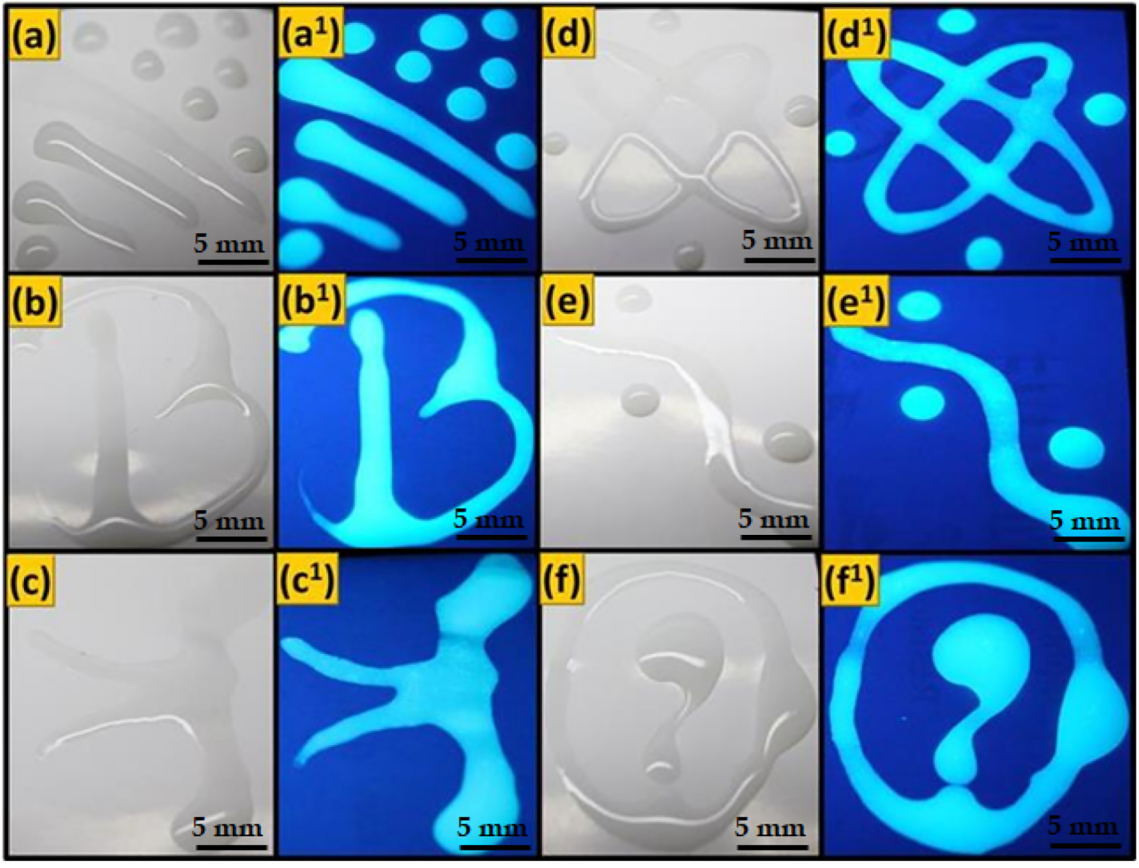
(a)
5 mm
(a¹)
5 mm
(d)
5 mm
(d¹)
5 mm
(b)
5 mm
(b¹)
5 mm
(e)
5 mm
(e¹)
5 mm
(c)
5 mm
(c¹)
5 mm
(f)
5 mm
(f¹)
5 mm

Figure 17